# Insight into charge/discharge behaviors of intercalation batteries: relation of delivered capacity versus applied rate and intercalation mechanism of multi-particle systems

Mohammad Mahdi Kalantarian*[a]1, Hatef Yousefi Mashhour[a], Hamideh Shahroudi[a],

Nasim Osanloo[a] and Piercarlo Mustarelli[b]

[a]*Ceramic department, Materials and Energy Reseach Centet, Tehran, Iran*

[b]*Department of Materials Science, University of Milano-Bicocca, Viale Cozzi 55, 20125 Milano, Italy. E-mail: piercarlo.mustarelli@unimib.it.*

.

* Corresponding author.
*E-mail address: kalantarian@gmail.com, m.kalantarian@merc.ac.ir*

# Electronic Supplementary Information

## Methodology

### Experimental details

$Li_2FeSiO_4$/C nano-composite was synthesized by sol-gel and solid-state reaction methods. In the sol-gel synthesis route, lithium acetate (Merck), iron(III) nitrate (Merck) and tetra-ethyl orthosilicate (TEOS, Aldrich) were used as pristine materials. Ethylene glycol (Merck) and citric acid (Merck) was added to TEOS in the 1:1/3:1 molar ratio. After 1 hr mixing via magnetic stirring, lithium acetate and then iron(III) nitrate were added to the solution, that was kept at rest overnight in order to obtain the sol. Then, it was dried at 80 $^oC$ for 24 hr, then grinded and calcinated in a horizontal silica tube furnace under the Argon atmosphere at 700 $^oC$ for 1 hr with a heating rate of 6 $^o$/min.

Solid-state reaction synthesis was performed via lithium silicate ($Li_2SiO_3$, CHEMOS), iron(III) oxide ($Fe_2O_3$, Aldrich) and glucose ($C_6H_{12}O_6$, Aldrich) as the carbon source for both carbon coating and reduction of iron(III) to iron(II). Two samples with different amounts of glucose, i.e. 19 %wt and 38 %wt, were prepared. The corresponding carbon *in-situ* amount in the synthesized powder was about 4 %wt and 8 %wt (samples named SS2 and SS1, respectively). The precursor materials were grinded in an agate mortar and calcinated at 700 $^oC$ for 7 hr. The heating rate was 6 $^oC$/min and 3 $^oC$/min for SS-8C and SS-16C samples, respectively.

The electrochemical tests were performed using a three-electrodes T-cell with stainless steel current collectors, lithium metal as the negative electrode and a glasswool (Whatman GF/A) disc as the separator.

* Corresponding author.
*E-mail address: kalantarian@gmail.com, m.kalantarian@merc.ac.ir*

The electrolyte was 1M $LiPF_6$ in ethylene carbonate/diethyl carbonate (EC/DEC) 1:1 (Merck). In order to prepare the cathode layer, a slurry was made by mixing the active material with carbon black (Alfa) and poly[vinylidene fluoride] (PVdF, Solvay) in N-methyl-2-pyrrolidone solvent (NMP, Aldrich) with a weight ratio of 80:10:10. The obtained suspensions were spread on an aluminum foil and dried at 80 $^oC$ overnight. The cell was assembled in a dry-box under argon atmosphere (MBraun, <1ppm $O_2$, <1ppm $H_2O$). The galvanostatic cycling tests were carried out at different current rates using an Arbin battery cycler (model BT2000), between 2 and 4.63 V at room temperature. Three charge-discharge measurements of SG are reported here. High-performance cell manufactured by SG powder is named SG1, and two low-performance batteries are named SG2 and SG3. For SG1 cell almost theoretical capacity was obtained at C/20 rate.

**Computational details**

All the calculations in this work were performed using full-potential linear augmented plane-wave (FP-LAPW) method as implemented in the WIEN2K code1 within the framework of density functional theory (DFT).2 Inside the non-overlapping spheres of mu□n tin radius ($R_{MT}$) around each atom, linear combination of radial solution of the Schrödinger equation times the spherical harmonics are used and the plane-wave basis set is used in the interstitial region. Calculations are reported for two categories of $R_{MT}$ values. For one $R_{MT}$ of Fe, Li, Si, and O were set at 2.00, 1.97, 1.42 and 1.42 a.u., respectively, hereinafter named $R_{Fe}$=2.0; and for the other was set at 1.75, 1.60, 1.42 and 1.42 a.u., respectively, hereinafter called $R_{Fe}$=1.75. To expand the wave functions in the interstitial region, the plane-wave cut-o□ value of $K_{max}.R_{mt}$ =7.0 was used. The Fourier expanded charge density was truncated at $G_{max}$=12 $(Ryd)^{1/2}$ . The maximum value of the angular momentum ($l_{max}$) was set equal to 10 for the wave function expansion inside the atomic spheres. The Convergence of the self-consistent iterations was performed within 0.0001 Ry.

The structure with $Pmn2_1$ space group suggested by Nytén et al.[3] was used as the initial structure for $Li_2FeSiO_4$ material. For all materials, calculations were carried out on fully relaxed structures. Relaxation was applied following three approaches: minimization of atomic positions (force set at 0.001 $Ry.au^{-1}$), optimization volume with constant a:b:c ratio and optimization volume with variable a, b and c for the orthorhombic structure.

For the assessment of structural and electrochemical properties the calculations were carried out using spin polarized Perdew–Burke–Ernzerhof of generalized gradient approximation (PBE-GGA),[4] and local (spin) density approximation (L(S)DA). Integrals were calculated over the Brillouin zone with k-points based on 4×5×5 Monkhorst–Pack (MP) mesh. This grade contains 50 k-points in the irreducible Brillouin zone. The electron and spin configurations are software defaults, and for Fe, Li, Si and O atoms are $Fe_{up}$: [Ar] $3d^{6.5}$(4.5↑, 2↓) $4s^{1.5}$(1↑, 0.5↓), Li: [He] $2s^1$, Si: [Ne] $3s^2$ $3p^2$ and O: [He] $2s^2$ $2p^4$, respectively. For more comprehensive results, the PBE-GGA and LDA plus an on-site Coulomb Self-Interaction Correction potential[5] ($U^{SIC}$) were employed, hereinafter called GGA+U and LDA+U, respectively. U value was set at 5 eV.[6] An important electrochemical property that can be assessed directly from the di□erence in total energies before and after lithium extraction is the theoretical voltage ($V_T$). This parameter is calculated in this study from charge reaction (20), and is described by Eq. (21):

$Li_2FeSiO_4 \rightarrow Li_xFeSiO_4 + (2\text{-}x)Li$ (20)

$$V_{T,2-x} = E_{Li_2FeSiO_4} - E_{Li_xFeSiO_4} - (2-x)E_{Li} \quad (21)$$

Where $E_{Li_2FeSiO_4}$, $E_{Li_xFeSiO_4}$ and $E_{Li}$ are the calculated total energies of one unit formula for lithiated, delithiated structures and lithium metal (bcc structure), respectively. To determine $E_{Li}$, relaxation process was carried out with optimization of volume, then total energy ($E_{Li}$) was calculated based on 3094 k-points in the irreducible Brillouin zone (50×50×50 grid) setting energy convergence at E=0.00001 Ry.

# Results Section

## 1. Relation between average obtained capacity and current rate (Eqn. 2 of the paper)

Noteworthy, here the mechanism of Figure 5 of the paper has to be supposed.

In Figure S1, $S_i$ and $S_j$ is the slope of high rate ($I_h$, for example, C/5) and low rate ($I_l$, for example, C/20) voltage-capacity (V-C) curvature in point $P_i$ and $P_j$ , respectively. Points $P_i$ and $P_j$ are in the same stage of the process (for example 30% of the process was progressed for both of which). In other words, $P_i$ and $P_j$ are the points located in one line in $\frac{\partial V}{\partial C} - \sqrt{rate}$ diagram (according to eq. s1). Many peer points and so many peer slopes (like $S_i$ and $S_j$) could be assumed to satisfy the relation.

Here, it is desired to select a parameter that can be used as a substitute for all the slopes in various points of the diagram.

$$\partial V/\partial C \approx a_4 E_r \sqrt{D^*}\sqrt{d}\frac{1}{\sqrt{C}} \quad (s1)$$

Eqn. S1 is the same as eqn. 2 in the paper. If "S" was slope of V-C curvature ($\frac{\partial V}{\partial C}$), "I" was applied current rate and interpretation of D* and the other parameters were constant (using one distinctive battery), then:

$$S = \alpha\sqrt{I} \quad (s2)$$

When $\alpha$ is a constant.

For point of $S_i$ in Figure S1:

$$S_i = \alpha\sqrt{I_l} \quad (s3)$$

Assuming n points like $P_i$ in curvature with rate of $I_l$, it will be n slopes like $S_i$ named:

$S_1, S_2 \ldots S_i, \ldots$ and $S_n$ (s4)

According to eq. s3:

$S_1 = \alpha\sqrt{I_l}$ , $S_2 = \alpha\sqrt{I_l}$ … $S_i = \alpha\sqrt{I_l}$ , … and $S_n = \alpha\sqrt{I_l}$ (s5)

Summing two sides of the above equations (eqs. s5):

$$\sum_{1}^{n} S_i = n\alpha\sqrt{I_l} \quad \text{(s6)}$$

$$\frac{1}{n}\sum_{1}^{n} S_i = \alpha\sqrt{I_l} \quad \text{(s7)}$$

We suppose that for each considered point ($p_i$) of the low rate ($I_l$) curve, there is a corresponding point in the high rate ($I_h$) diagram, named $p_j$. Slopes of the curvature in the points are named as:

$S_1, S_2 \ldots S_j \ldots S_n$ (s8)

And so:

$$\frac{1}{n}\sum_{1}^{n} S_j = \alpha\sqrt{I_h} \quad \text{(s9)}$$

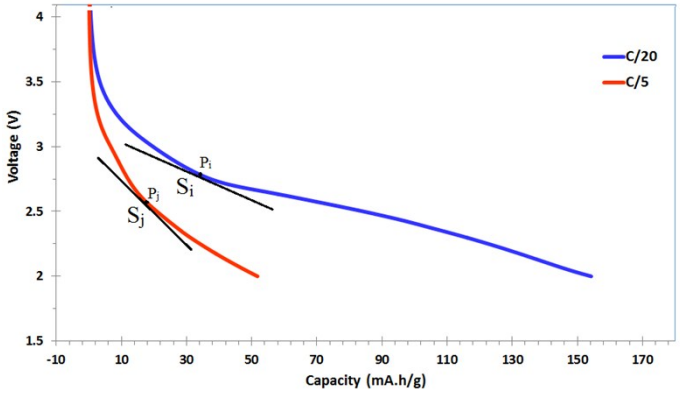


**Figure S1.** Voltage vs. capacity (V-C) discharge diagrams for a $Li_2FeSiO_4$ sample (as an example). $S_i$ and $S_j$ is the slope of the curvature supposed to be in the same discharge state for low (C/20) and high (C/5) rate, respectively.

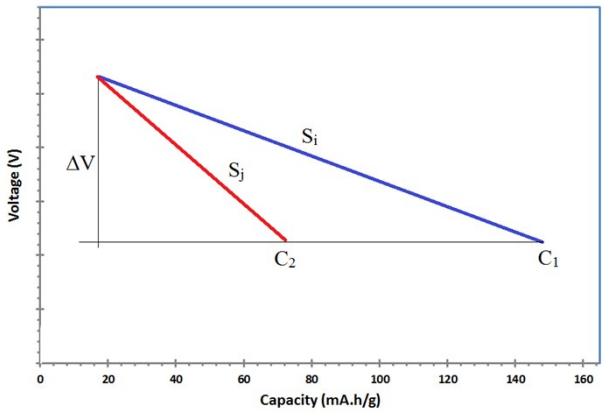


**Figure S2.** Drawing of Si and Sj slopes of Figure S1 in triangles to evaluate their relation.

According to Figure S2:

$$S_i = \frac{\Delta V}{C_1} = \frac{\Delta V}{a_i \bar{C}_l} = \frac{b_i}{\bar{C}_l} \qquad \text{(s10)}$$

$$S_j = \frac{\Delta V}{C_2} = \frac{\Delta V}{a_j \bar{C}_h} = \frac{b_j}{\bar{C}_h} \qquad \text{(s11)}$$

When ΔV, $C_1$ , and $C_2$ are as shown in Figure S2; $\bar{C}_l$ and $\bar{C}_h$ is ultimate obtained capacity for low and high rate measurement, respectively; $a_i$ and $a_j$ are fraction of progressing of the process which they was assumed to be equal (for example 30%); so, $b_i$ and $b_j$ (as constants) would be equal. Consequently, $\sum_1^n b_i = \sum_1^n b_j = B$. Let's assume $B/n^2$ is equal to another constant named A.

$$\frac{1}{n}\sum_1^n S_i = \frac{\sum b_i}{n^2 \bar{C}_l} = \frac{B}{n^2 \bar{C}_l} = \frac{A}{\bar{C}_l} \qquad \text{(s12)}$$

$$\frac{1}{n}\sum_1^n S_j = \frac{\sum b_j}{n^2 \bar{C}_h} = \frac{B}{n^2 \bar{C}_h} = \frac{A}{\bar{C}_h} \qquad \text{(s13)}$$

When A and B are constants. Using eqs. s7 and s9, eqs. s12 and s13 will turn to eqs. s14 and s15, respectively.

$$\frac{A}{\bar{C}_l} = \alpha\sqrt{I_l} \qquad \text{(s14)}$$

$$\frac{A}{C_h} = \alpha\sqrt{I_h} \qquad \text{(s15)}$$

Therefore, the relation between $^{1}/_{C}$ and square root of the corresponding rate is linear for both of eqns. S14 and s15, and therefore they are in the same line for both supposed rates. Here, $C$ was the ultimate obtained capacity of one cycle. If the measurement was applied for many cycles, obviously, average obtained capacity could be used.

Noteworthy, the mechanism of Figure 5 was supposed for the above calculations. Therefore, validity of the approved relation (as it was established in Figure 1-4 of the paper) is an additional evidence for approval of suggested mechanism in Figure 5.

## 2. Additional information for Figure 4 of the paper

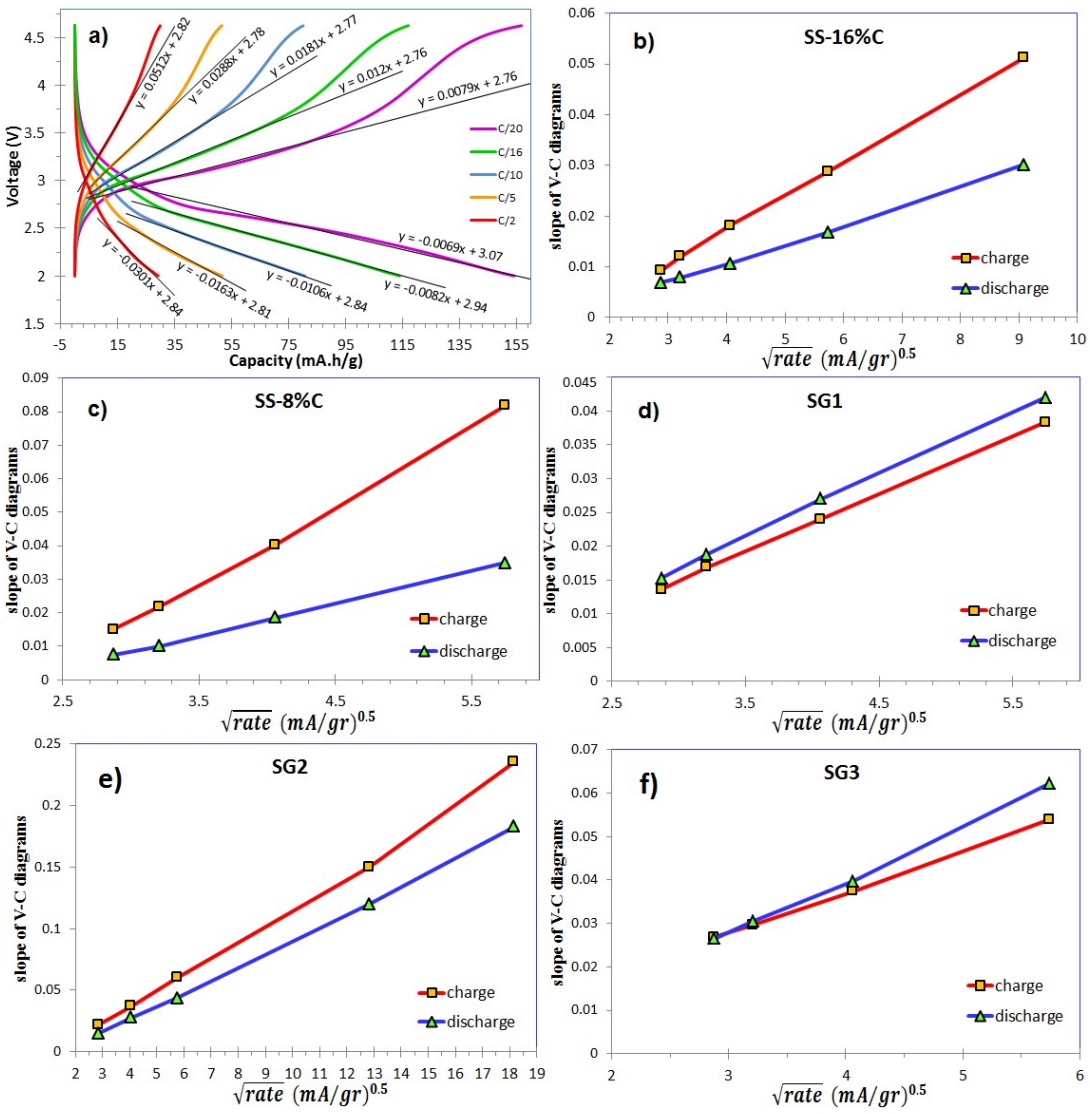


**Figure S3.** a) An example for the region that the slopes were taken from for Figure 4 of the paper. The diagrams are charge and discharge diagrams of SS1 sample for different applied rates (mA/gr), best linear fits and their equations are shown. b), c), d), e) and f) slope of voltage-capacity (V-C) diagrams versus square root of applied rate (mA/gr) for charge and discharge processes of SS1, SS2, SG1, SG2 and SG3 measurements, respectively.

## 3. Electronic conductivity of lithiated, delithiated, intermediate and interface phases of $Li_2FeSiO_4$

Figure S4 shows the calculated density of states (DOS) diagrams for the intermediate, interface, lithiated and delithiated phases of $Li_2FeSiO_4$, intended as a case study. According to our results, electron conductivity of intermediate ($Li_{1.5}FeSiO_4$) and interface ($Li_{0.5}FeSiO_4$ and $FeSiO_4$) phases are higher than that of lithiated ($Li_2FeSiO_4$) and delithiated ($LiFeSiO_4$) phases.

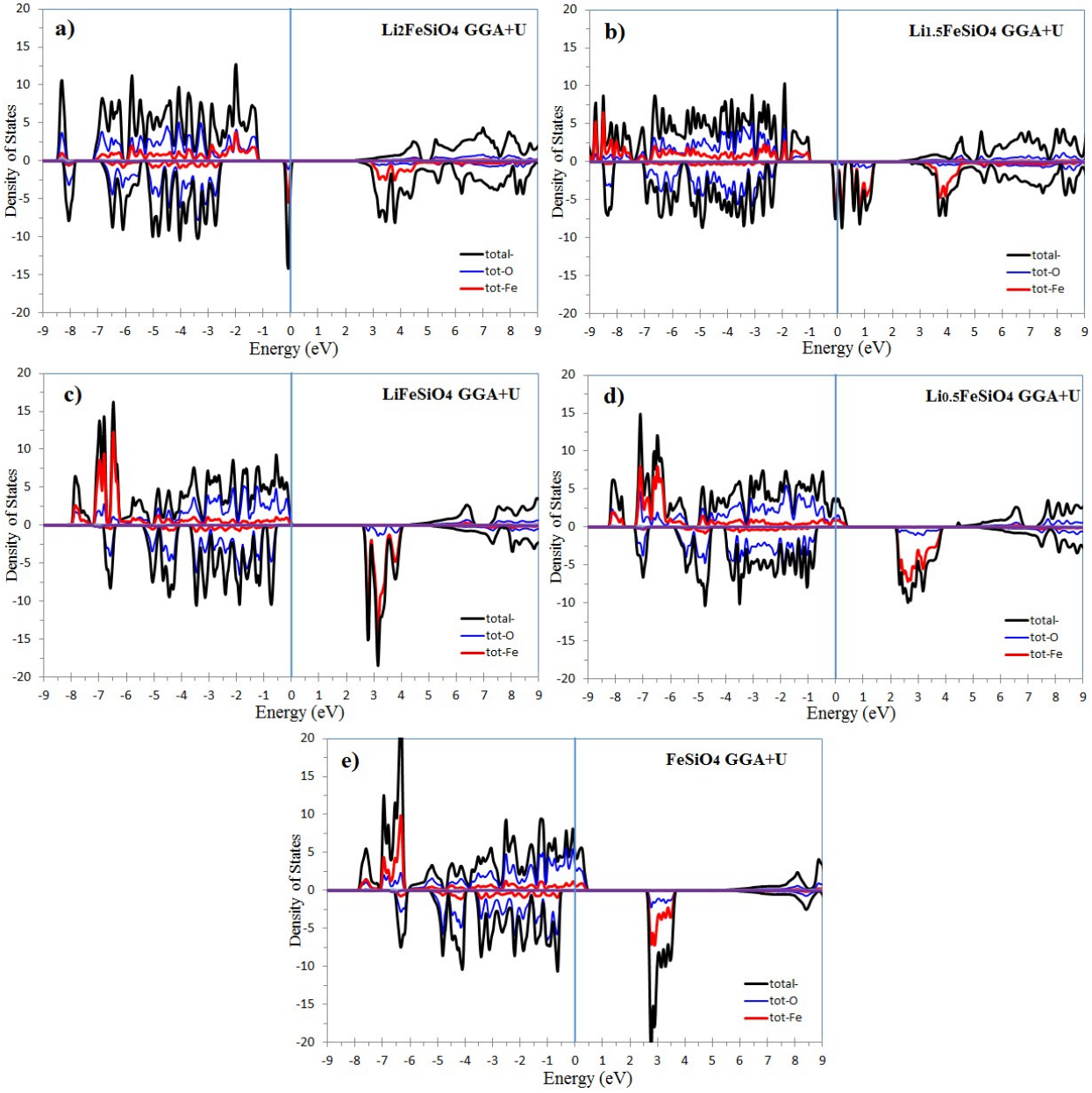


**Figure S4.** Calculated density of states (DOS) by GGA+U ($R_{Fe}$=2) method[7] for a) $Li_2FeSiO_4$ as lithiated phase, b) $Li_{1.5}FeSiO_4$ as intermediate phase, c) $LiFeSiO_4$ as delithiated phase, d) $Li_{0.5}FeSiO_4$ as interface phase and e) $FeSiO_4$ as interface phase. Fermi level is set at zero.

## 4. Beyond "rate restricted by Li mobility" condition.

Let's consider $Li_2FeSiO_4$ as a case study. The conclusion will be the same for the other cathode materials, because the rational is the same.

In the case of $Li_2FeSiO_4$ discharge process (Figure S5-a), reactant is $LiFeSiO_4$ (delithiated phase) and the reaction product is $Li_2FeSiO_4$ (lithiated one). The average formula of the intermediate phase is

$Li_{1.5}FeSiO_4$. Therefore, as shown in Figure S5-a, Li diffusion takes place through $Li_2FeSiO_4$. Diffusion process of Li in $Li_{1.5}FeSiO_4$ is easier than in $Li_2FeSiO_4$, because one of the four Li positions is empty. Therefore, the Li mobility restriction holds for $Li_2FeSiO_4$ and not for $Li_{1.5}FeSiO_4$. Consequently, during discharge, restriction of Li mobility in lithiated phase ($Li_2FeSiO_4$) would cause the intermediate phase width to increase.

In the case of $Li_2FeSiO_4$ charge process (Figure S5-b), the reactant is $Li_2FeSiO_4$ (lithiated phase) and the product of the reaction is $LiFeSiO_4$ (delithiated one). Intermediate and interface phases are supposed to be $Li_{1.5}FeSiO_4$ and $Li_{0.5}FeSiO_4$, respectively. As shown in Figure S5-b, diffusion process takes place through $Li_{1.5}FeSiO_4$-$LiFeSiO_4$-$Li_{0.5}FeSiO_4$ regions. Diffusion of Li would be easier in $Li_{0.5}FeSiO_4$ (interface) than into $LiFeSiO_4$ (delithiated) and $Li_{1.5}FeSiO_4$ phases. Therefore, restriction of Li mobility will not limit expansion of the interface region as an alternative product of delithiation. The expansion of the interface region is enough to assure the model validity under this condition. Moreover, by increasing $Li_{0.5}FeSiO_4$ (interface) amount, increasing of $Li_{1.5}FeSiO_4$ (intermediate) is also expected due to the reaction

$$Li_{1.5}FeSiO_4 + Li_{0.5}FeSiO_4 \rightarrow 2LiFeSiO_4$$

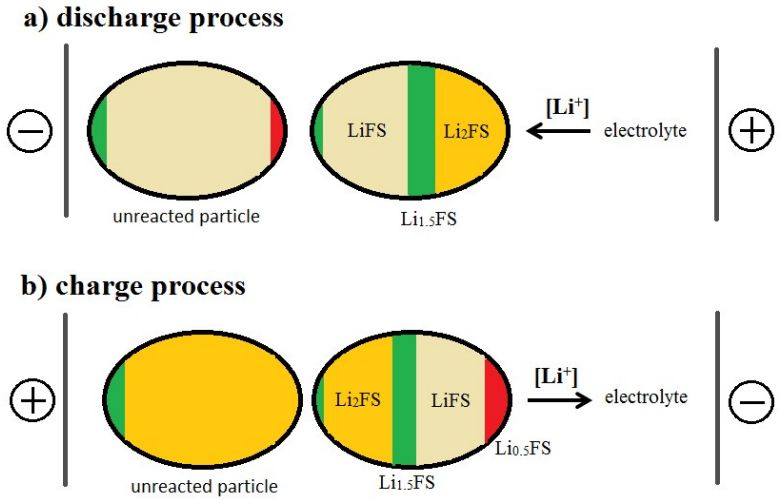


**Figure S5.** Schematic illustration of discharge (lithiation, a) and charge (delithiation, b) processes to show the relative location of intermediate/interface phases with respect to the lithiated/delithiated ones.

## 5. "Charge" companion of Figure 5.

Figure 5 in the paper showed our suggested mechanism for discharge process. Figure S6 shows the same mechanism for charge process.

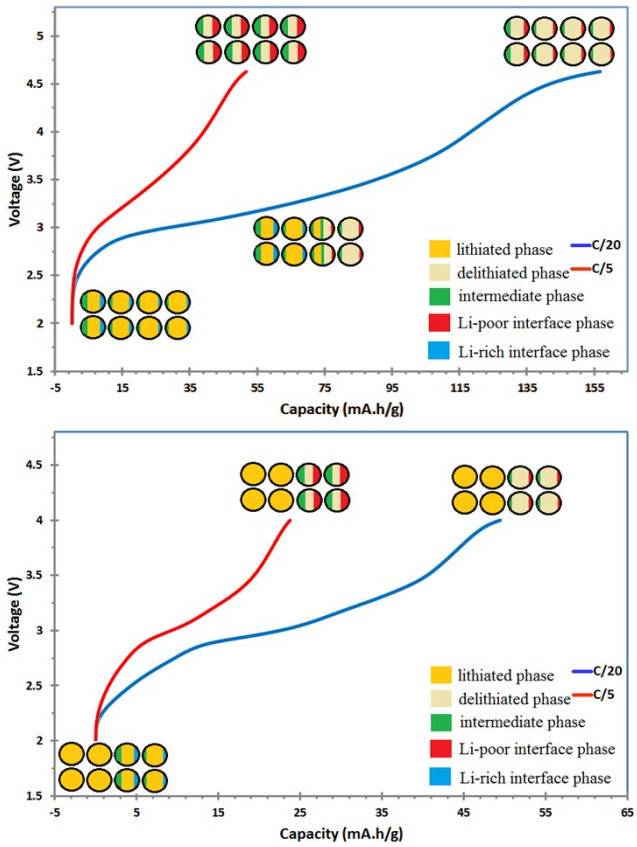


**Figure S6.** Companion of Figure 5 for charge process. It illustrates schematic delithiation process at different rates (after the first cycle) according to the mechanism suggested in ref. [7] for: a) For a high capacity sample (like SS1 or SG1) and b) For delivering low capacities even at low rates (SG2 or SG3). In this scenario, the low obtained capacity in the case of b) is caused by low depth of discharge, i.e. a lower number of particles participate to the electrochemical process. Also, low obtained capacity at high rate is caused by high amount of intermediate/interface phases. In the case of $Li_2FeSiO_4$, the average value of x in $Li_xFeSiO_4$ formula is about 1.5 and 0.5 for intermediate and interface phases, respectively,[7] and Li-rich interface is the same of the lithiated phase.

## 6. Details on the mechanism sketched in Figure 5

When low capacity was obtained, it means that all the particles or/and their entire fractions are not reacted (de/intercalated) completely. In other words, since capacity is correlated to the effective mass of the cathode when the ultimate (theoretical) capacity was not obtained, it means that the supposed cathode active mass is not (de)lithiated completely. This can take place for two reasons: a) a number of particles did not participate in the process, and/or b) all of the particles participated, but the resulting phase was not completely reacted phase (intercalated/deintercalated phase).

In order to investigate decreasing of the capacity by increasing the rate, Figure S7 shows a good performance cell (high capacity at low rates and low capacity at high rates). Both of the possible above scenarios (Figure S7-a and S7-b) and the combination of them (Figure S7-c) are illustrated in the figure. We will discuss these three possible situations.

Figure S7-a illustrates that the intercalation process at high rate would perform in the same manner of low rates but with less depth of discharge. In this scenario, the capacity would be declined but voltage of cell will not be agreed with the resulted phases. Assuming that cell voltage is related to the potential of the reacted phases (Gibbs phase law), Figure S7-a is not correct. Otherwise speaking, in Fig. S7-a scenario our model [7] would not be governed, however, we established in the paper that the results are accommodated with the model.

In the case of $Li_2FeSiO_4$ cathode material (as an example), $LiFeSiO_4$, $Li_{1.5}FeSiO_4$ and $Li_2FeSiO_4$ should be considered as delithiated, intermediate and lithiated phase, respectively. Calculated theoretical cell voltage of $Li_2FeSiO_4/LiFeSiO_4$ is ~3.1 V and for $Li_2FeSiO_4/Li_{1.5}FeSiO_4$ is about 1.5 V.[7] Therefore, in the cut-off voltage (2 V) reacted phase should be a combination of $Li_{1.5}FeSiO_4$ , and $LiFeSiO_4$ compounds. At high voltage (i.e. ~2.75 V), the amount of $Li_{1.5}FeSiO_4$ phase should be less than at low voltage (i.e. ~2.0 V).

Figure S7-b shows the case when depth of discharge at low rates is the same that at high rates, but in the case of low rates intermediate region is progressed for all the particles. This suggestion could satisfy both capacity and voltage values, and also in terms of eq. s1 all the slopes would be located along the same line because the mechanism would not be changed. Subsequently, this scenario was chosen as the governed mechanism (Figure 5 of the paper).

Just to complete the discussion, Figure S7-c shows combination of Figure S7-a and S7-b. In this figure depth of discharge for high rates is less than that for low rates (a number of particles have remained inactive for high rates). Also, the last delithiated particles contained high amount of intermediate phase ($Li_{1.5}FeSiO_4$) to satisfy the cut-off voltage. This scenario is not possible because of two reasons. If this scenario was correct: a) the curve at high rate (i.e. C/5) would behave as the curve at low rate (i.e. C/20) and then would decline suddenly to the cut-off voltage, b) for the suggested eq. s1 all the slopes would not be located along the same line because the mechanism would be changed.

Based on the above discussions, Figure S7-b was selected as the suggested mechanism and reported as Figure 5a of the paper.

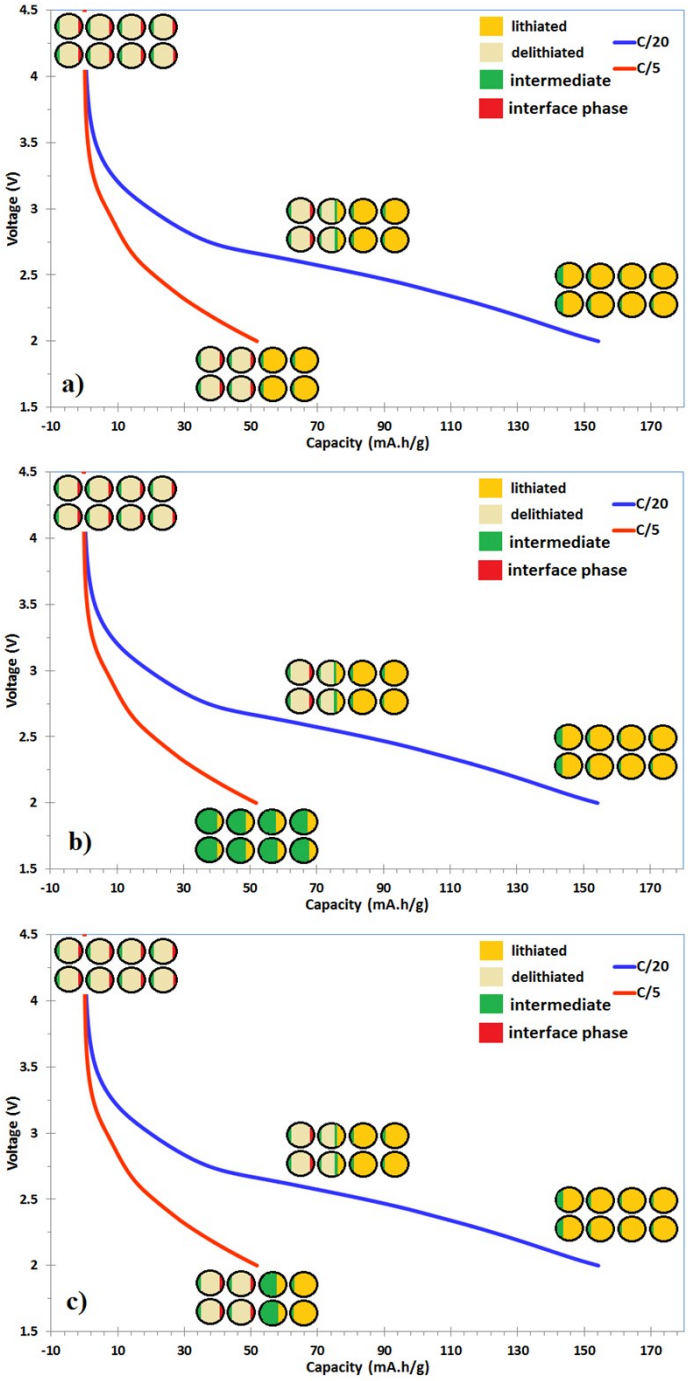


**Figure S7.** Alternative mechanisms for decreasing capacity upon increasing the rate. V-C curves of a cathode that resulted in a good performance cell. For $Li_2FeSiO_4$, lithiated, delithiated, intermediate and interface phases are $Li_2FeSiO_4$, $LiFeSiO_4$, $Li_{1.5}FeSiO_4$ and $Li_{0.5}FeSiO_4$, respectively.

In the case of low-performance cells (low capacity even at low rates, e.g. SG2 and SG3 cells), two scenarios are possible, which are sketched in Figure S8.

If all the particles were active (Figure S8-b) then the theoretical capacity would be obtained at least at low current rates (i.e. C/20), but it was not the case. We used the same powder for the measurement named SG1, SG2, and SG3. Noteworthy, absolute values of current rate (mA) for SG2 were lower than SG1 (at C/20 they were $6.9\times10^{-3}$ versus $7.1\times10^{-3}$ mA, respectively), but the obtained capacity was higher for SG1. Therefore, it could be concluded that only a fraction of the particles was active in such a case (which means a lower depth of discharge/charge). Subsequently, Figure S8-a should then be correct and proposed as the suggested mechanism in Figure 5b of the paper. In the case of high performance, obviously, the mechanism sketched in Figure S7-b (Figure 5a) should be considered.

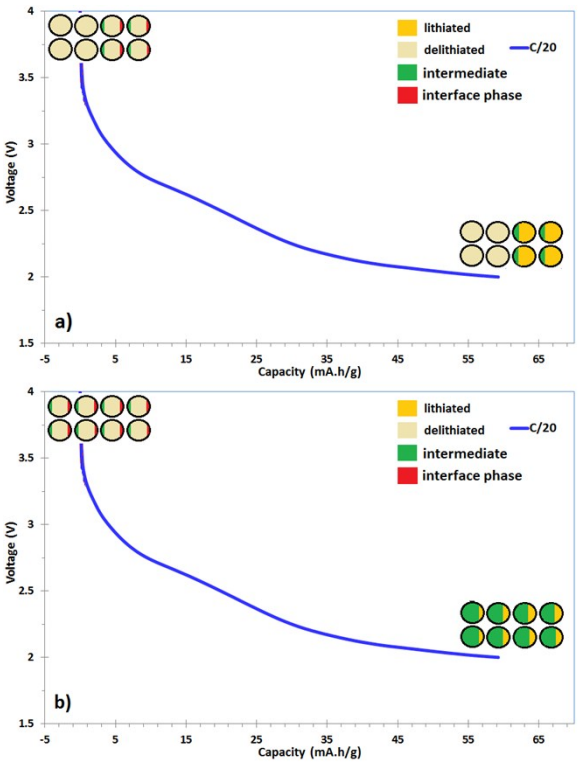


**Figure S8.** Alternative mechanisms for the low performance condition (low capacity even at low rates) obtained by SG2 and SG3-based cells.

## 7. Regarding cuspid in lines of $1/C - \sqrt{rate}$ chart

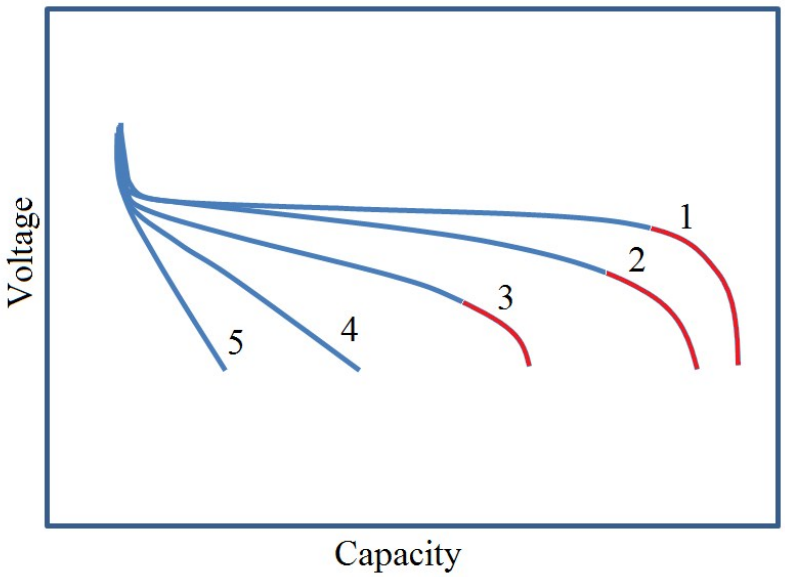


**Figure S9.** Scheme of V-C diagram for different applied rates (the rate is increasing from 1 to 5). Curvatures 1, 2 and 3 have the same nature of undesired[7] (bipolarizing)[8, 9] phase relevant to red parts of the curves. For 4 and 5 curves reaching cut-off voltage would avoid origination of the undesired phase (the red part of curves). Therefore, from 3 to 4, nature of undesired phase is changed. In such a case, there would be a cuspid in the relevant line of $1/C - \sqrt{rate}$ chart (points corresponding to 1, 2 and 3 would be occurred in one line and 4 and 5 in another one.).

## 8. Trend-lines of Figures 2 and 3

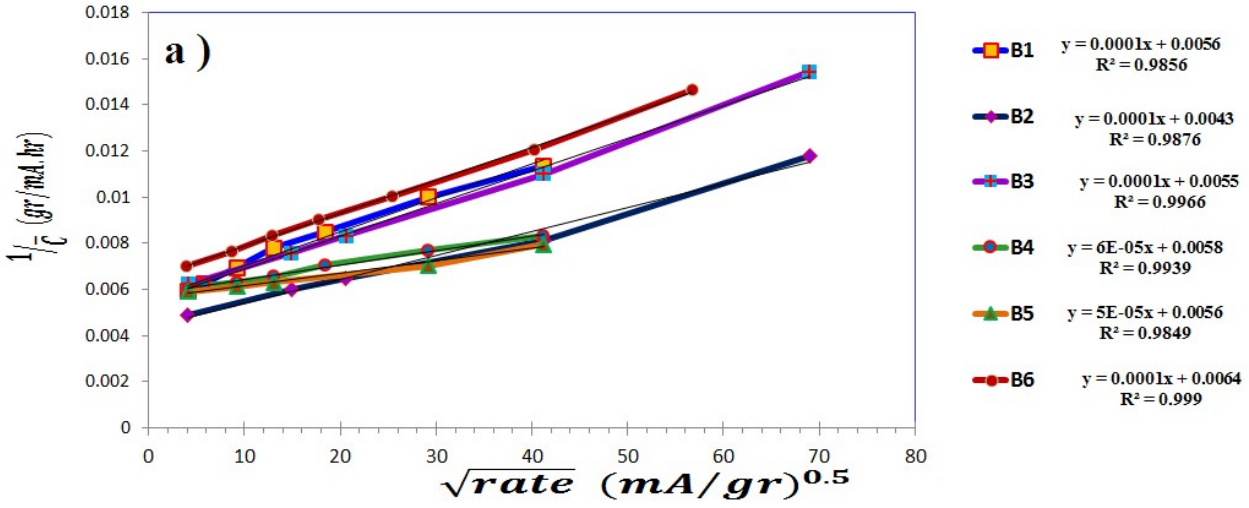
a )
0.018
0.016
0.014
0.012
0.01
0.008
0.006
0.004
0.002
0
0
10
20
30
40
50
60
70
80
1/C (gr/mA.hr)
√rate (mA/gr)^0.5
B1 y = 0.0001x + 0.0056 R² = 0.9856
B2 y = 0.0001x + 0.0043 R² = 0.9876
B3 y = 0.0001x + 0.0055 R² = 0.9966
B4 y = 6E-05x + 0.0058 R² = 0.9939
B5 y = 5E-05x + 0.0056 R² = 0.9849
B6 y = 0.0001x + 0.0064 R² = 0.999

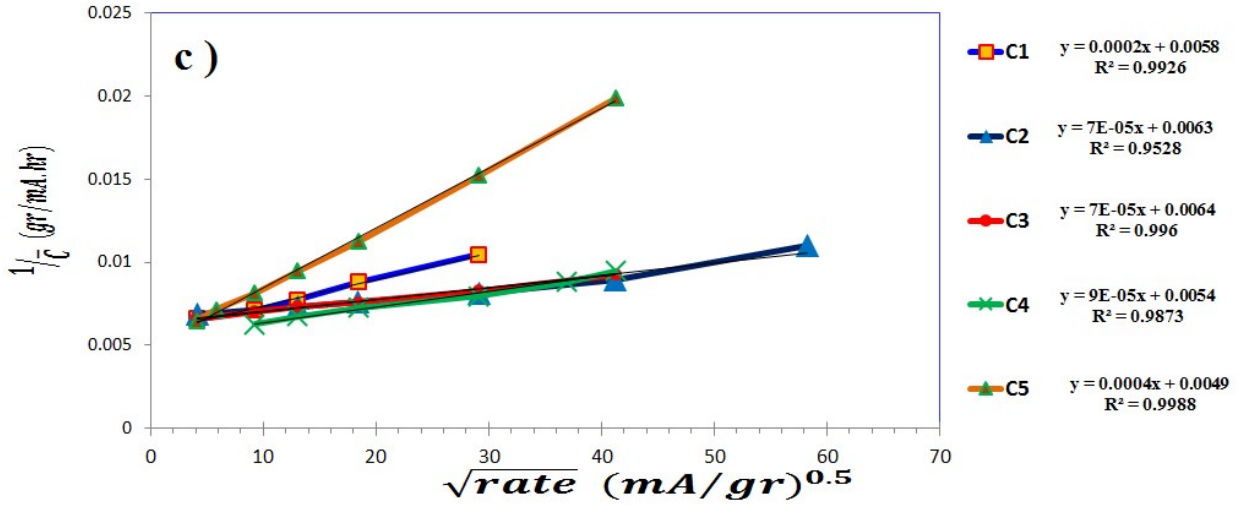
c )
0.025
0.02
0.015
0.01
0.005
0
0
10
20
30
40
50
60
70
1/C (gr/mA.hr)
√rate (mA/gr)^0.5
C1 y = 0.0002x + 0.0058 R² = 0.9926
C2 y = 7E-05x + 0.0063 R² = 0.9528
C3 y = 7E-05x + 0.0064 R² = 0.996
C4 y = 9E-05x + 0.0054 R² = 0.9873
C5 y = 0.0004x + 0.0049 R² = 0.9988

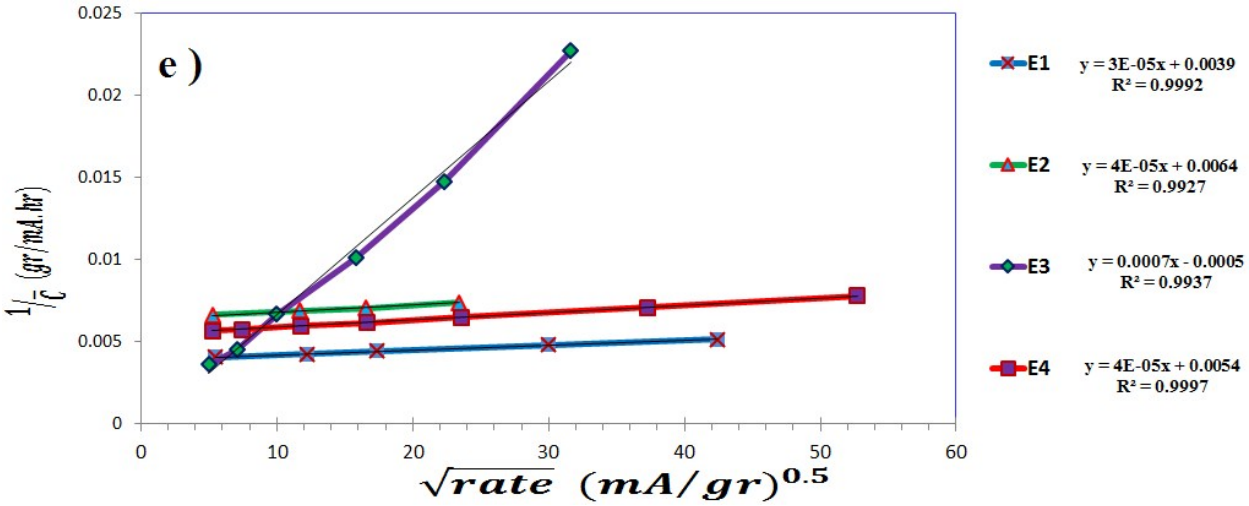
e )
0.025
0.02
0.015
0.01
0.005
0
0
10
20
30
40
50
60
1/C (gr/mA.hr)
√rate (mA/gr)^0.5
E1 y = 3E-05x + 0.0039 R² = 0.9992
E2 y = 4E-05x + 0.0064 R² = 0.9927
E3 y = 0.0007x - 0.0005 R² = 0.9937
E4 y = 4E-05x + 0.0054 R² = 0.9997

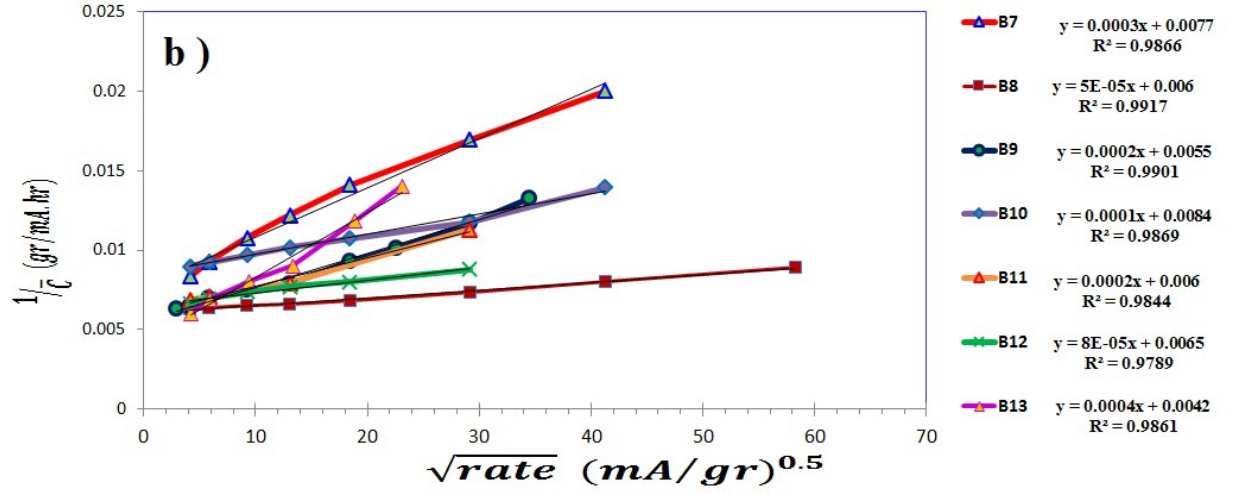
b )
1/t (gr/mA.hr)
√rate (mA/gr)^0.5
B7 y = 0.0003x + 0.0077 R² = 0.9866
B8 y = 5E-05x + 0.006 R² = 0.9917
B9 y = 0.0002x + 0.0055 R² = 0.9901
B10 y = 0.0001x + 0.0084 R² = 0.9869
B11 y = 0.0002x + 0.006 R² = 0.9844
B12 y = 8E-05x + 0.0065 R² = 0.9789
B13 y = 0.0004x + 0.0042 R² = 0.9861

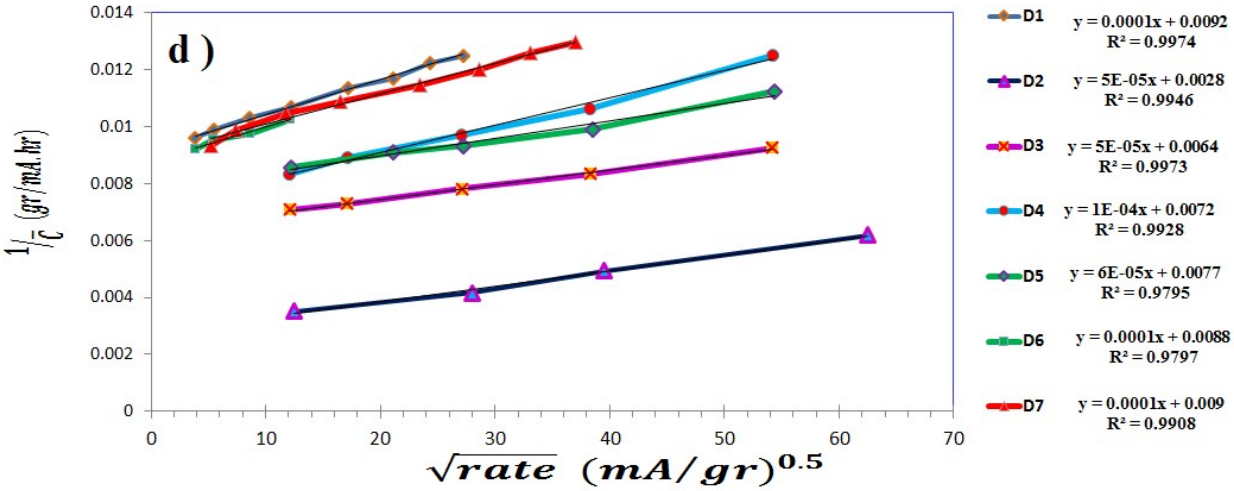
d )
1/t (gr/mA.hr)
√rate (mA/gr)^0.5
D1 y = 0.0001x + 0.0092 R² = 0.9974
D2 y = 5E-05x + 0.0028 R² = 0.9946
D3 y = 5E-05x + 0.0064 R² = 0.9973
D4 y = 1E-04x + 0.0072 R² = 0.9928
D5 y = 6E-05x + 0.0077 R² = 0.9795
D6 y = 0.0001x + 0.0088 R² = 0.9797
D7 y = 0.0001x + 0.009 R² = 0.9908

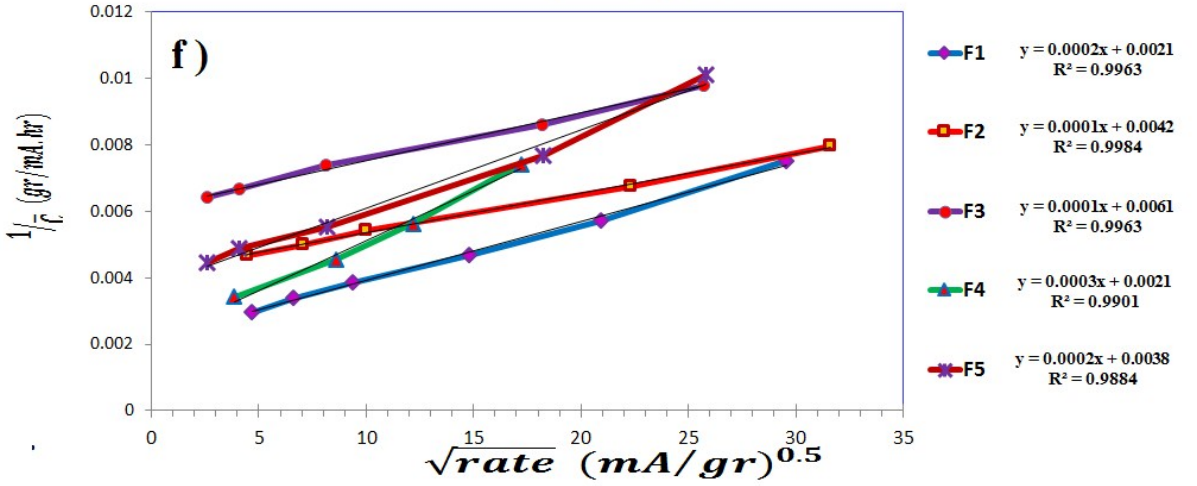
f )
1/t (gr/mA.hr)
√rate (mA/gr)^0.5
F1 y = 0.0002x + 0.0021 R² = 0.9963
F2 y = 0.0001x + 0.0042 R² = 0.9984
F3 y = 0.0001x + 0.0061 R² = 0.9963
F4 y = 0.0003x + 0.0021 R² = 0.9901
F5 y = 0.0002x + 0.0038 R² = 0.9884

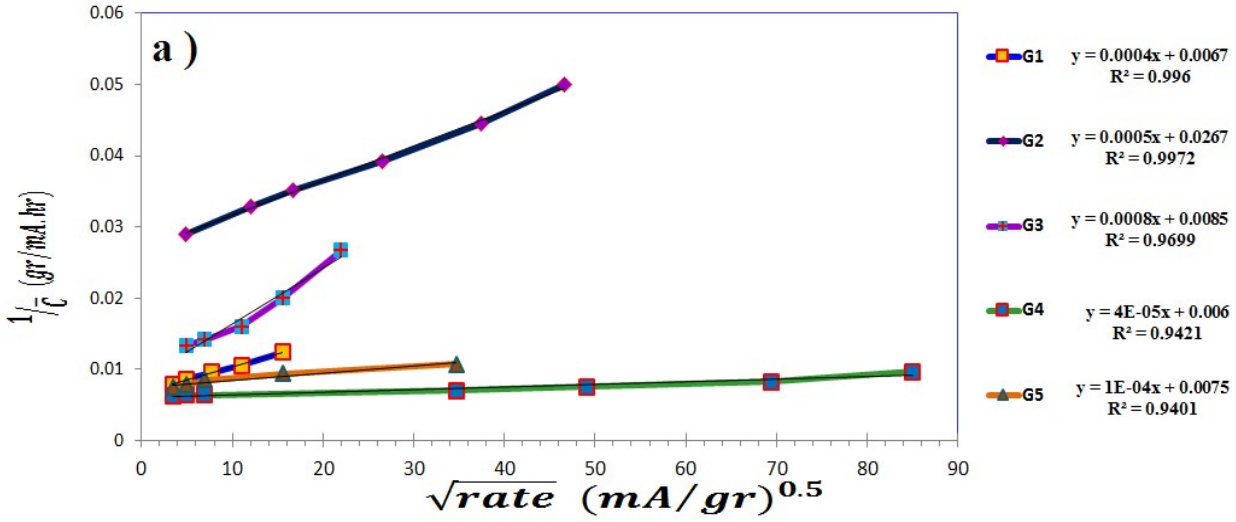
a )
0.06
0.05
0.04
0.03
0.02
0.01
0
0
10
20
30
40
50
60
70
80
90
$\frac{1}{C}$ (gr/mA.hr)
$\sqrt{rate}$ $(mA/gr)^{0.5}$
G1 y = 0.0004x + 0.0067 R² = 0.996
G2 y = 0.0005x + 0.0267 R² = 0.9972
G3 y = 0.0008x + 0.0085 R² = 0.9699
G4 y = 4E-05x + 0.006 R² = 0.9421
G5 y = 1E-04x + 0.0075 R² = 0.9401

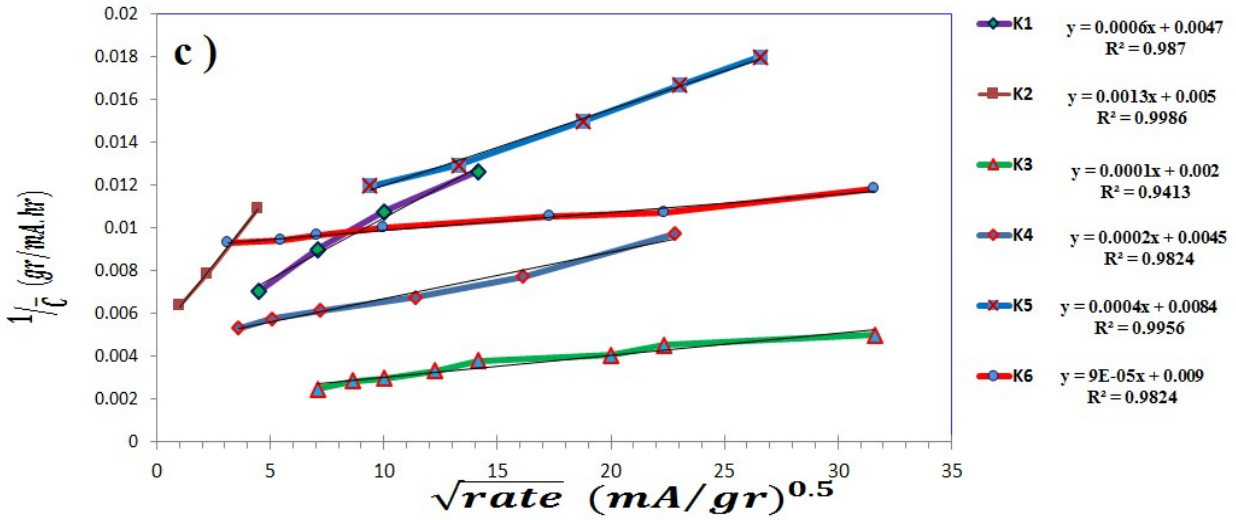
c )
0.02
0.018
0.016
0.014
0.012
0.01
0.008
0.006
0.004
0.002
0
0
5
10
15
20
25
30
35
$\frac{1}{C}$ (gr/mA.hr)
$\sqrt{rate}$ $(mA/gr)^{0.5}$
K1 y = 0.0006x + 0.0047 R² = 0.987
K2 y = 0.0013x + 0.005 R² = 0.9986
K3 y = 0.0001x + 0.002 R² = 0.9413
K4 y = 0.0002x + 0.0045 R² = 0.9824
K5 y = 0.0004x + 0.0084 R² = 0.9956
K6 y = 9E-05x + 0.009 R² = 0.9824

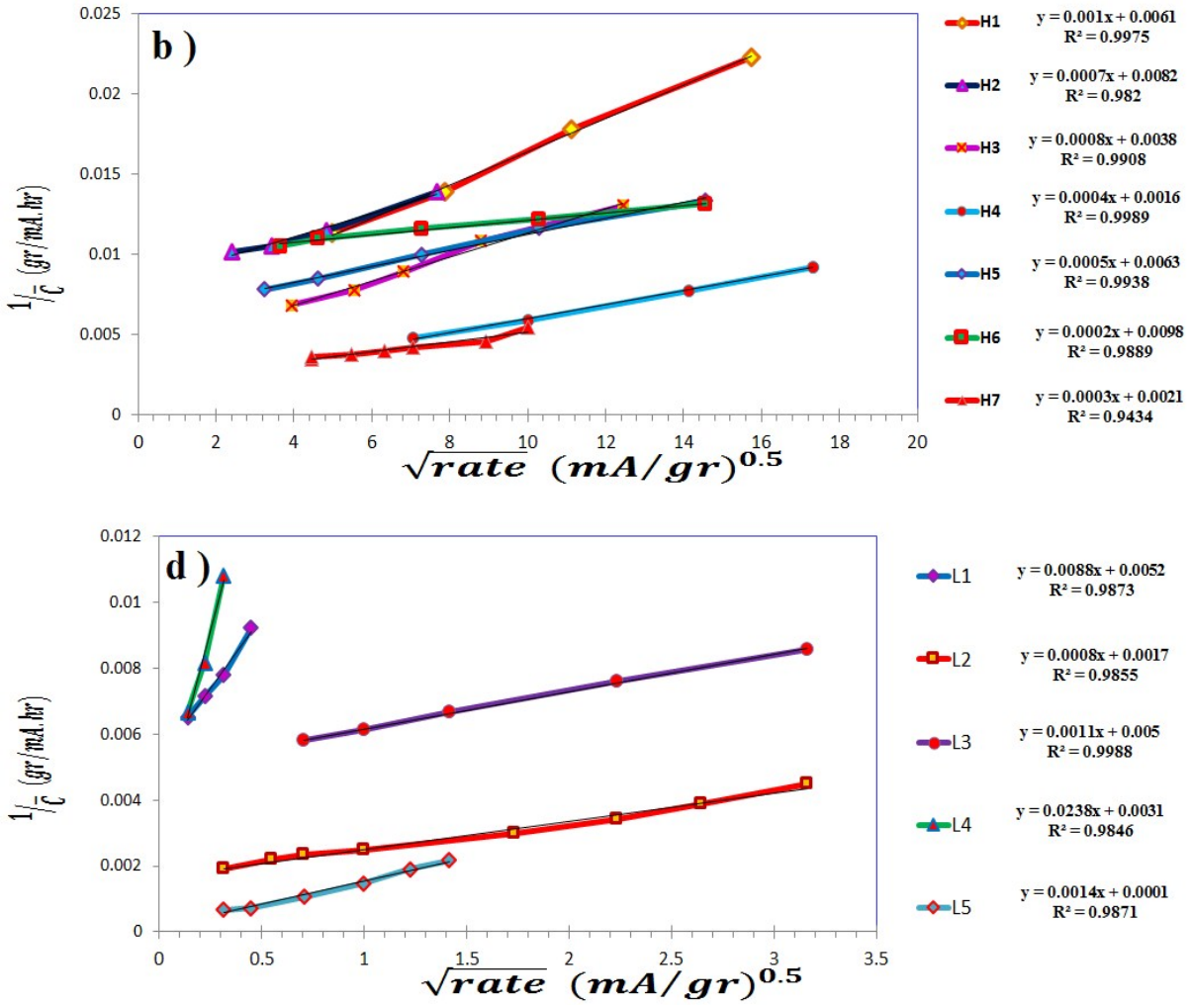


## Reference


1. P. Blaha, K. Schwarz, G. Madsen, D. Kvasnicka and J. Luitz, *WIEN2k, An augmented plane wave plus local orbitals program for calculating crystal properties*, Vienna University of Technology, Austria, Austria, 2001.
2. P. Hohenberg and W. Kohn, *Physical review*, 1964, 136, B864.
3. A. Nytén, A. Abouimrane, M. Armand, T. Gustafsson and J. O. Thomas, *Electrochemistry communications*, 2005, 7, 156-160.
4. J. P. Perdew, K. Burke and M. Ernzerhof, *Physical review letters*, 1996, 77, 3865.
5. V. Anisimov, I. Solovyev, M. Korotin, M. Czyżyk and G. Sawatzky, *Physical Review B*, 1993, 48, 16929.
6. M. M. Kalantarian, S. Asgari, D. Capsoni and P. Mustarelli, *Physical Chemistry Chemical Physics*, 2013, 15, 8035-8041.
7. M. Kalantarian, M. Oghbaei, S. Asgari, S. Ferrari, D. Capsoni and P. Mustarelli, *Journal of Materials Chemistry A*, 2014, 2, 19451-19460.

8. M. M. Kalantarian and H. Yousefi Mashhour, *in press*, 2019.
9. M. M. kalantarian and H. Yousefi Mashhour, *in press*, 2019.